



A new lidar inversion method using a surface reference target. Application to the backscattering coefficient and lidar ratio retrievals of a fog-oil plume at short-range

Florian Gaudfrin^{1,2,3}, Olivier Pujol², Romain Ceolato¹, Guillaume Huss³, and Nicolas Riviere¹

¹ONERA / DOTA, Université de Toulouse, F-31055 Toulouse - France

²Université de Lille, Département de physique, Laboratoire d'optique atmosphérique, 59655 Villeneuve d'Ascq, France

³LEUKOS, 37 rue Henri Giffard, 87280 Limoges, France

Correspondence: Florian Gaudfrin (florian.gaudfrin@onera.fr)

Abstract. In this paper, a new elastic lidar inversion equation is presented. It is based on the backscattering signal from a surface reference target (SRT) rather than that from a volumetric layer of reference (Rayleigh molecular scatterer) as usually done. The method presented can be used when the optical properties of such a layer are not available, *e.g.* in the case of airborne elastic lidar measurements or when the lidar-target line is horizontal. Also, a new algorithm is described to retrieve the lidar ratio and the backscattering coefficient of an aerosol plume without any *a priori* assumptions about the plume. In addition, our algorithm allows a determination of the instrumental constant. This algorithm is theoretically tested, *viz.* by means of simulated lidar profiles, and then using real measurements. Good agreement with available data in the literature has been found.

1 Introduction

Atmospheric aerosols are liquid or solid particles dispersed in the air (Glickman and Zenk, 2000) of natural (volcano, biomass burnings, desert, ocean...) or anthropogenic origins. They play an important role in cloud formation (DeMott et al., 2010), radiative forcing (Hansen et al., 1997)(Hay, 2000) and more generally for researches on the climate change, but also in the context of air quality and public health (Bal, 2008; Finlayson-Pitts and Pitts, 2000; Popovicheva et al., 2019; Zhang et al., 2018). Their size varies from the nanometer to the millimeter scale (Robert, n.d.). However, a large majority of aerosols have a size between $0.01 \mu\text{m}$ and $3 \mu\text{m}$ (Clark and Whitby, 1967) for which scattering is dominant in the optical domain. The Mie theory is often used, at least statistically (*i.e.* for a large population of random sized aerosols), although aerosols are not always spherical. The optical backscattering and extinction properties of aerosols are mainly related to their shape (Ceolato et al., 2018), size distribution (Vargas-Ubera et al., 2007), concentration and chemical composition which is based to their nature (dust, maritime, urban). Lidar are active remote sensing instruments suitable for aerosol detection and characterization (Sicard et al., 2002) over kilometric distances during both day and nighttime.



The optical properties of aerosols are obtained by means of inversion methods using the simple scattering lidar equation. In the 1980s, a stable one-component formulation adapted to lidar applications was proposed by Klett (1981). It has then been extended to a two-component formulation, *viz.* separating molecular and aerosol contributions, by Fernald (1984) and Klett (1985). The elastic lidar equation is an ill-posed problem in the sense of Hadamard (1908) since one searches for extinction and for backscattering coefficients with only a single observable. Several assumptions are therefore required in order to invert the lidar equation:

- (i) A calibration constant is usually determined from a volumetric layer of the upper atmosphere as a reference target (Vande Hey, 2014). This volume is considered made only of pure molecular constituents whose optical scattering properties are well-known (Rayleigh regime). The molecular backscattering coefficient is generally estimated from the standard model of the atmosphere (Anon, 1976; Bodhaine et al., 1999). However, poor estimates of the reference or low signal-to-noise ratios (SNR) can lead to severe uncertainties on the retrieved extinction and backscattering coefficients. Few sensitivity studies have been performed to evaluate such uncertainties (Matsumoto and Takeuchi, 1994; Rocadenbosch et al., 2012). Spatial averaging around the volume of reference in addition to time averaging is thus recommended to increase SNR .
- (ii) Lidar ratio is constant over the distance range of measurements (Sasano et al., 1985). This is also a source of important errors in the retrieval values. Some studies have proposed a variable lidar ratio under the form of a power-law relationship between the extinction and backscattering coefficients, but such a method requires an *a priori* knowledge of the medium under study (Klett, 1985).
- (iii) The molecular contribution along the lidar-line is known. It is estimated, as for the backscattering coefficient, by means of temperature and pressure vertical profiles, using either the standard model of the atmosphere or radio soundings (Jäger, 2005).

In the case of elastic lidar inversion, the most critical parameter is the lidar ratio (LR). It depends on the wavelength (in vacuum) and on the microphysics, morphology, and size of the particles (Hoff et al., 2008). The LR ranges from 20 sr to 100 sr at 532 nm (Ackermann, 1998; Cat, 2005; Leblanc et al., 2005) according to the aerosol origins (maritime, urban, dust particles, biomass burning). It is therefore difficult to assume an *a priori* value for LR in as much this information is to be found rather than given.

Several alternatives have been analyzed to constrain the inversion procedure while relaxing assumption (ii). These alternatives are based on the determination of the optical thickness, the one which consists in coupling lidar and sunphotometer measurements being the most largely used. The measured optical thickness is then used to constrain extinction profiles (Fernald et al., 1972; Pedrós et al., 2010). A second alternative, consists in combining elastic lidar and Raman measurements in order to get the optical depth as a function of range (Ansmann et al., 1990, 1992, 1997; Mattis et al., 2004). In a third technique, the optical depth is retrieved from elastic lidar measurements with different zenith angles (Sicard et al., 2002). It is worth indicating that coupling lidar and sunphotometer measurements is possible only daytime while Raman measurements are carried out preferentially at nighttime in order to increase the SNR .



Another limitation of lidar measurements is related to the overlap function that strongly impacts (and prevents) observation
55 close to the instrument, *i.e.* in the lowest layers of the troposphere where aerosols are emitted. Different studies have proposed to
modify the overlap function analytically (Comeron et al., 2011; Halldórsson and Langerholc, 1978; Kumar and Rocadenbosch,
2013; Stelmazczyk et al., 2005) or empirically (Vande Hey et al., 2011; Wandinger and Ansmann, 2002). Some lidar devices
are also equipped with a second telescope of higher overlap at short range (Ansmann et al., 2001). However, current lidar
systems are not adapted enough to the monitoring and characterization of volumetric targets at short-range, for instance in the
60 industrial context, or more generally, for anthropogenic activities (Ceolato and Gaudfrin, 2018).

To meet new industrial emission control requirements and very recently emitted anthropogenic aerosols characterization, we
have developed a short-range lidar of high spatial resolution (Gaudfrin et al., 2019)(Gaudfrin et al., 2018b). The lidar inversion
cannot be performed by means of the classical Klett-Fernald equation, because the reference layer used for the inversion
is either impossible to access (horizontal lidar measurements, sky-to-ground lidar airborne measurements), or inaccessible
65 because of finite lidar range. In the present paper, a modification of the conventional lidar equation is proposed in order to
perform lidar inversions using a surface reference target (SRT) at relatively short range ($r_{max} \approx 100$ m). Precisely, a unified
lidar equation for surface and volumetric scattering media is suggested, and it is then used for a new inversion equation,
inspired from the Klett-Fernald equation, using a SRT. Also a new technique to retrieve the lidar ratio without using any
sunphotometer or Raman measurements is presented and applied to an aerosol plume. This new inversion technique is both
70 assessed theoretically and experimentally using real lidar measurements. A discussion and a conclusion follow and close the
present paper.

2 Unified lidar equation for surface and volumetric scattering media

Currently, lidar inversion methods use a volumetric layer of the upper atmosphere (higher than 8 km of altitude above ground
level) as a reference target. This volume is considered as being free of aerosols and made only of pure molecular constituents
75 whose optical scattering properties are known. In our approach, we propose to use a SRT of known bidirectional reflectance
distribution function (BRDF) $f_{r,\lambda}$. In the sequel, the SRT is supposed to be Lambertian and so $f_{r,\lambda}(\theta_i) = \rho_\lambda \cos \theta_i / \pi$, with ρ_λ
the spectral reflectivity and θ_i (in rad) the angle between the normal eigenvector to the SRT and the incident beam direction.
This requires to modify the usual lidar equation to make it suitable for both surface and volumetric targets.

For the single-scattering lidar equation, for which light has undergone only one scattering event, the measured backscattered
80 power, at range r , can be written in a general way, *viz.* by considering both a surface target (Bufton, 1989; Hall and Ageno,
1970) and a volumetric target (Collis and Russell, 1976), as:

$$\mathcal{P}_\lambda(r, \theta_i) = \mathcal{P}_{p,\lambda} \frac{c\tau_\lambda}{2} \frac{A_{ef}}{r^2} \left\{ \beta_\lambda(r) + \frac{2}{c\tau_\lambda} f_{r,\lambda}(r_s, \theta_i) F_{cor} \right\} T_\lambda^2(r) \xi_\lambda(r) \eta_\lambda \quad (1)$$

where $\mathcal{P}_{p,\lambda}$ (in W) is the peak power of the laser source, $c \approx 3 \times 10^8$ m · s⁻¹ the Einstein's constant, τ_λ (in s) the laser pulse
duration (full width at half maximum), and A_{ef} (in m²) the telescope effective receiving area. Also, the SRT is located at
85 range r_s , ξ_λ the dimensionless overlap function, η_λ the dimensionless optical efficiency of the whole receiver, and T_λ^2 the back



and forth atmospheric transmission throughout the environment between the lidar source and range r (Swinehart, 1962):

$$T_\lambda(r) = \exp \left[- \int_0^r \alpha_\lambda(x) dx \right] \quad (2)$$

α_λ (in m^{-1}) being the total extinction coefficient at wavelength λ , and range r : $\alpha_\lambda = \alpha_{b,\lambda} + \alpha_{a,\lambda}$. The subscripts “b” and “a” refer, respectively, to the contribution of the background (molecules, aerosols) and to the contribution of the aerosol volumetric target under investigation. The total backscattering coefficient β (in $\text{m}^{-1} \cdot \text{sr}^{-1}$) is $\beta_\lambda = \beta_{b,\lambda} + \beta_{a,\lambda}$, with the same meaning as just above for the subscripts. By definition, the corresponding lidar ratios are $LR_{b,\lambda}(r) = \alpha_{b,\lambda}/\beta_{b,\lambda}$ and $LR_{a,\lambda}(r) = \alpha_{a,\lambda}/\beta_{a,\lambda}$, respectively.

In Eq.1, $\mathcal{P}_{p,\lambda}$ is conventionally a square-shaped pulse, *viz.* the ratio between the pulse energy and τ_λ . In the case of lidar measurements on a SRT, the backscattered peak-power is not proportional to $\mathcal{P}_{p,\lambda}$. A corrective factor F_{cor} depending on the real shape of the laser pulse is thus introduced. In the present case: $\mathcal{P}_{p,\lambda}^G = \mathcal{P}_{p,\lambda}^s F_{cor}$, with $\mathcal{P}_{p,\lambda}^G$ and $\mathcal{P}_{p,\lambda}^s$ the peak power of a Gaussian-shaped and a square laser pulse, respectively. Conservation of the pulse energy between these two kind of pulses gives $F_{cor} = 2(\ln 2/\pi)^{1/2}$. The fundamental quantity measured by the lidar instrument is a voltage V (in volts) which is proportionnal to the backscattered power: $V_\lambda(r) = R_{v,\lambda} \mathcal{P}_\lambda(r)$, where $R_{v,\lambda}$ is the detection constant (in $\text{V} \cdot \text{W}^{-1}$) which determines the light-voltage conversion. It can be written using the instrumental constant: $C_{ins} = R_{v,\lambda} K_s$ (in $\text{V} \cdot \text{m}^3$), where $K_s = \mathcal{P}_{p,\lambda} c \tau_\lambda A_{ef} \eta / 2$. In the literature, C_{ins} is obtained from \mathcal{P}_λ while, herein, it comes from the voltage and therefore takes into account all the emission, collection, detection and acquisition chain.

In the sequel, for better readability, the subscript λ and θ_i will not be written thereafter.

The range corrected lidar signal $V_\lambda(r)r^2$ is so:

$$S(r) = C_{ins} \left(\beta_a(r) + \beta_b(r) + f_r \frac{2}{c\tau} F_{cor} \right) \exp \left\{ -2 \int_0^r [\alpha_a(x) + \alpha_b(x)] dx \right\} \quad (3)$$

To remove the α -dependence in the exponential term, we will replace α_a and α_b by LR_a and LR_b , respectively, and introduce the term:

$$LR_a(r) \exp \left\{ -2 \int_0^r \beta_b(x) [LR_a(x) - LR_b(x)] dx \right\} \quad (4)$$

as detailed in Ansmann and Müller (2004). With such modifications, the final lidar equation for surface and volumetric scatterers can thus be written as:

$$S(r) LR_a(r) \exp \left\{ -2 \int_0^r \beta_b(x) [LR_a(x) - LR_b(x)] dx \right\} = C_{ins} \left[Y(r) + LR_a(r) \frac{2f_r}{c\tau} F_{cor} \right] \exp \left[-2 \int_0^r Y(x) dx \right] \quad (5)$$

with $Y(r) = LR_a(r) [\beta_b(r) + \beta_a(r)]$.



Thereafter, in order to highlight the expression to solve, it is convenient to define background corrected transmission factor:

$$D(0, r) = \exp \left\{ -2 \int_0^r \beta_b(x) [LR_a(x) - LR_b(x)] dx \right\} \quad (6)$$

and $W(r) = S(r)LR_a(r)D(r)$. Finally, Eq. 3 becomes:

$$115 \quad W(r) = C_{ins} \left[Y(r) + LR_a(r) \frac{2f_r}{c\tau} F_{cor} \right] \exp \left[-2 \int_0^r Y(x) dx \right] \quad (7)$$

We will now introduce the lidar framework adapted to the radiative parameter retrieval of a volumetric scattering medium with a known SRT.

3 New lidar inversion technique

3.1 Radiative parameters identification

120 The current Klett-Fernald inversion method consists in determining C_{ins} using the high atmosphere as a reference and to fix the LR_a a priori. In this paper, C_{ins} is determined by means of a SRT located at range r_s . So:

$$C_{ins} = \frac{c\tau}{2f_r F_{cor}} W(r_s) \frac{1}{LR_a(r_s)} \exp \left[2 \int_0^{r_s} Y(x) dx \right] \quad (8)$$

It is worth mentioning that $LR_a(r_s)$ is the lidar ratio just before the SRT. Also, obviously, for $r < r_s$, $f_r = 0$. Inserting Eq. 8 in Eq. 7 gives:

$$125 \quad W(r) = \frac{c\tau}{2f_r F_{cor}} \frac{W(r_s)}{LR_a(r_s)} Y(r) \exp \left[2 \int_r^{r_s} Y(x) dx \right] \quad (9)$$

This equation can be solved by integrating both sides from r to r_s (Vande Hey, 2014). The exponential term is (see Appendix):

$$\exp \left[2 \int_r^{r_s} Y(x) dx \right] = 1 + \frac{4f_r F_{cor} LR_a(r_s)}{c\tau W(r_s)} \int_r^{r_s} W(x) dx \quad (10)$$

Plugging Eq. 10 into Eq. 9, we obtain in the following:

$$130 \quad Y(r) = W(r) \left[\frac{c\tau W(r_s)}{2f_r F_{cor} LR_a(r_s)} + 2 \int_r^{r_s} W(x) dx \right]^{-1} \quad (11)$$

Using the definitions of $Y(r)$ and $W(r)$ (see above), $\beta_a(r)$ can be written as:

$$\beta_a(r) = S(r)D(0, r) \left[\frac{c\tau S(r_s)D(0, r_s)}{2f_r F_{cor}} + 2 \int_r^{r_s} S(x)LR_a(x)D(0, x) dx \right]^{-1} - \beta_b(r) \quad (12)$$



Multiplying the numerator and the denominator of the first term on the right-hand side by $D(0, r_s)$, this expression becomes:

$$\beta_a(r) = S(r)D(r_s, r) \left[\frac{c\tau S(r_s)}{2f_r F_{cor}} + 2 \int_r^{r_s} S(x)LR_a(x)D(r_s, x) dx \right]^{-1} - \beta_b(r) \quad (13)$$

135 Then, by definition of the lidar ratio, we deduce $\alpha_a(r) = LR_a(r)\beta_a(r)$. Eq. 13 is similar to the one defined by Klett (1981), except that β_b in Eq. 13 contains also the contribution of the aerosol background.

Assuming that the properties of the SRT are well known, the most critical parameter is $LR_a(r)$. Giving a value for LR_a requires an *a priori* knowledge of the volumetric target under study whereas the main objective of lidar remote sensing is precisely to characterize the medium investigated. *A priori*s are always topic of discussions and are more or less severe flaws
 140 in lidar measurements.

Equation 13 can also be applied on the important context of airborne observations. In this case, it is necessary to know the ground *BRDF*.

3.2 Determination of LR_a and β_a : methodology

The objective is to retrieve first $\beta_a(r)$ and LR_a (and then to deduce $\alpha_a(r)$) without any *a priori* about the medium considered.
 145 Two lidar measurements are performed: the first one (signal V_s) in the absence of the volumetric aerosol medium of interest and a subsequent one (signal V_{sv}) in its presence. The SRT is obviously present for both measurements. The two measurements should be performed close in time in order to avoid that the background environment evolves too much. The experimental setup of these lidar measurements is illustrated on Fig. 1

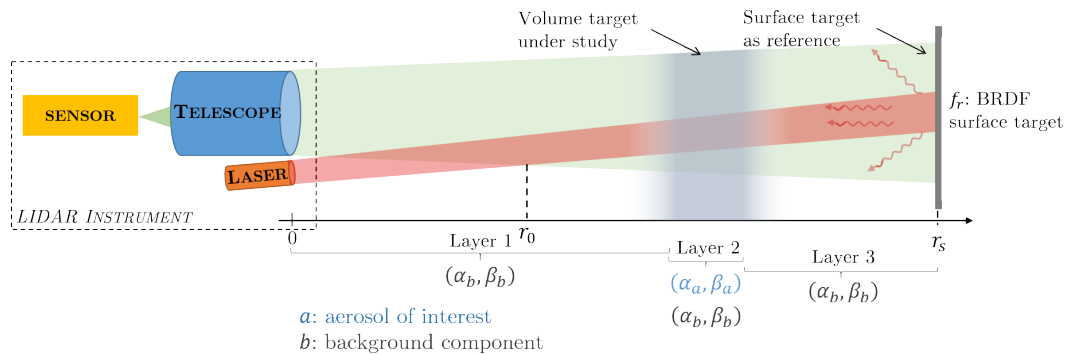


Figure 1. Illustration of the experimental setup

By definition, the half-logarithmic ratio of S_s and S_{sv} corresponds to the total extinction of the volumetric media under
 150 study: $\alpha_{tot} = \ln[S_s(r_s)/S_{sv}(r_s)]/2$. Using S_s , C_{ins} can be determined independently of the volumetric medium of interest:

$$C_{ins} = \frac{c\tau}{2f_r F_{cor}} S_s(r_s) \exp \left[2 \int_0^{r_s} \alpha_b(x) dx \right] \quad (14)$$



which is Eq. 8 with $\alpha_a = 0$. C_{inst} and α_{tot} are used in objective functions to retrieve LR_a , assumed to be uniform – r –independent. The first objective function is:

$$\varepsilon_1 = \left| \int_{r_0}^{r_s} \alpha_a(x) dx - \alpha_{tot} \right| \quad (15)$$

155 where α_a is the retrieved profile of extinction using Eq. 13 and LR_a . The medium is assumed to be at range of full overlap ($r > r_0$), so that α_{tot} must correspond to the integrated extinction. A second objective function:

$$\varepsilon_2 = \left| \int_{r_0}^{r_s} [S_{sv}(x) - S_{sim}(x)] dx \right| \quad (16)$$

is introduced in order to minimize the difference between S_{sv} and the simulated signal S_{sim} obtained from the retrieved β_a and α_a and from C_{inst} .

160 The methodology is presented on Fig. 2. The molecular background contribution is computed from pressure and temperature data as in Bucholtz (1995), while the aerosol background contribution is estimated by means of radiative transfer codes, e.g. MATISSE (Simoneau et al., 2002; Labarre et al., 2010) or MODTRAN (Berk et al., 2008, 2014). Another solution consists in using a realistic value of the visibility \mathcal{V} (in km^{-1}) and the Koschmieder's relation (Horvath, 1971; Elias et al., 2009; Hyslop, 2009) at 550 nm (maximum human eye sensitivity): $\mathcal{V}\alpha_b \approx 3.9$

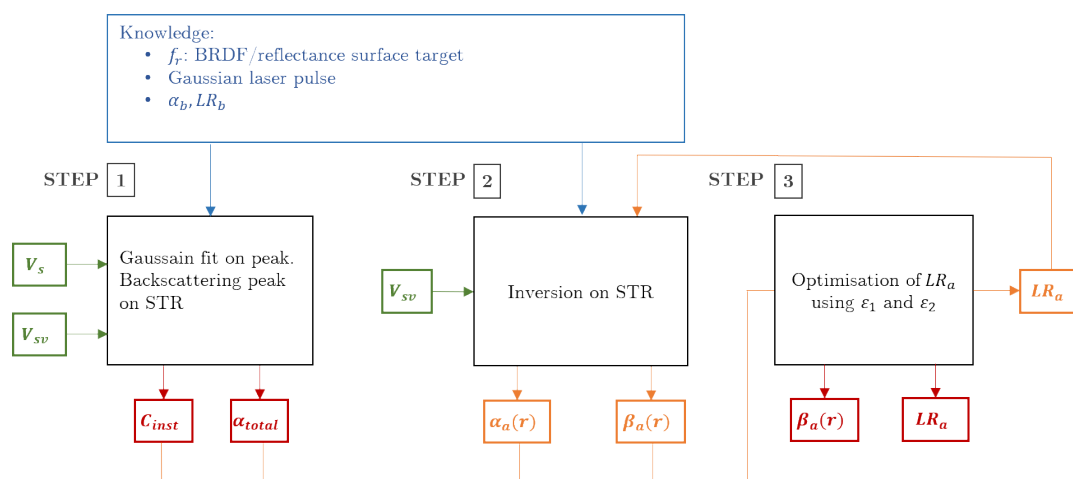


Figure 2. Diagram illustrating how the inversion algorithm allows to retrieve the $\beta_a(r)$ and LR_a without assumptions on the volume medium of interest. In green the lidar signals inputs, in orange the intermediate calculations during the optimization procedure and in red the code outputs.

165 The signals V_s and V_{sv} are introduced in the inversion procedure, which is organized around three main steps (Fig. 2):

1. A Gaussian fit is first applied on the backscattered signal from the SRT, i.e. $V_s(r_s)$ and $V_{sv}(r_s)$, that gives the amplitude of the backscattering, the position of this peak and its width in position. From these gaussian models, one can obtain α_{tot}



(from its definition, see above) and C_{ins} from Eq. 14. Note: When the target is tilted with respect to the lidar-target line, the backscatter peak of surface target will not be symmetrical. An other fit should be used as a log-normal function.

- 170 2. A first lidar inversion is realized using Eq. 13 with $LR_a = 50$ sr at the beginning of the inversion procedure. This value has been chosen because it corresponds to the average LR_a data of the literature. For that, the gaussian model V_{sv} obtained at step 1 is used for signal $S(r_s)$ in Eq. 13. A first range-profile $\beta_a(r)$ is thus obtained at the end of this second step.
- 175 3. The above $\beta_a(r)$ and LR_a allow to determine $\alpha_a(r)$ whose r -integration is then compared with α_{tot} in the minimization procedure of Eq. 15. At each iteration, the LR_a is modified in order to reduce ε_1 . The new $\beta_a(r)$, LR_a , and so $\alpha_a(r)$ are then used to compute a simulated lidar signal S_{sim} whose comparison with S_{sv} is minimized according to Eq. 16. In this algorithm, the iterative procedure ends up when $\varepsilon_1 + \varepsilon_2 \leq 10^{-6}$ is reached. A number of 19 iterations is generally enough, depending on the first value of LR_a introduced initially (step 2). At the end of this step, one thus obtains final $\beta_a(r)$, $\alpha_a(r)$ and LR_a . The minimization procedure used is the one implemented by Kraft (1988). Eq. 15 is the most
- 180 important since it determines the rapidity of convergence. Eq. 16 is helpful but not critical.

4 Theoretical behavior of the retrieval procedure

4.1 Theoretical lidar signals

The inversion method described above is tested using theoretical lidar signals generated by PERFALIS¹ (Gaudfrin et al., 2018a). As summarized in Table 1, the simulated atmosphere is composed of three layers and of a SRT of BRDF $f_r =$
185 $0.20/\pi$ located at $r_s = 100$ m. Pressure and temperature are uniform (1040hPa and 290K) and the continental aerosol background is chosen so that it corresponds to $\mathcal{V} = 47$ km (Hess et al., 1998). In addition, $\beta_b = 1.05 \times 10^{-5} \text{ m}^{-1} \cdot \text{sr}^{-1}$ and $LR_b = 51.01$ sr. The signal V_s is generated from the background components and the SRT, while the signal V_{sv} is generated considering an aerosol plume aerosol between 20 – 30m (second layer). The plume backscatter coefficient is $\beta_a = 7.14 \times 10^{-5} \text{ m}^{-1} \cdot \text{sr}^{-1}$ and $LR_a = 70$ sr. Multiple scattering is assumed to be negligible. For dense atmosphere and
190 wider field of view, Eq. 1 has to be corrected by an appropriate factor (Bissonnette, 1996) in order to consider higher orders of scattering events.

¹PERFORMANCE Assessment for LIdar Systems



	Notation	Layer 1	Layer 2	Layer 3	SRT ($f_r = 0.20/\pi \text{ sr}^{-1}$)
Range	r (in m)	0 – 20	20 – 30	30 – 100	100
Background components	α_b (in m^{-1})	1.18×10^{-3}	1.18×10^{-3}	1.18×10^{-3}	X
	β_b (in $\text{m}^{-1} \cdot \text{sr}^{-1}$)	9.97×10^{-6}	9.97×10^{-6}	9.97×10^{-6}	
	LR_b (in sr)	118.56	118.56	118.56	
Volumetric medium	α_a (in m^{-1})	X	5.00×10^{-3}	X	X
	β_a (in $\text{m}^{-1} \cdot \text{sr}^{-1}$)		7.14×10^{-5}		
	LR_a (in sr)		70		

Table 1. Input optical parameters of the scene used in the lidar simulator (PERFALIS code) as illustrated on Fig. 1

Inversion methods are generally applied to averaged signals in order to increase the SNR . In lidar remote sensing, the noise can be, approximately, considered as a white Gaussian noise (Li et al., 2012; Mao et al., 2013; Sun, 2018). In order to assess the impact of noise in the inversion method (see Section 3), a Gaussian noise of null mean value and a standard deviation of 1.5×10^{-5} a.u. is introduced in the theoretical lidar signals. Figure 3 displays the theoretical noised signals V_s and V_{sv} . As expected, because of light extinction by the plume, $V_{sv}(r_s)$ is lower than $V_s(r_s)$ by 9%. Four datasets are then generated, with respectively, an averaging over 20, 50, 100, and 200 signals, from V_s and V_{sv} , and, in addition, a fifth signal without noise is considered (Fig. 4).

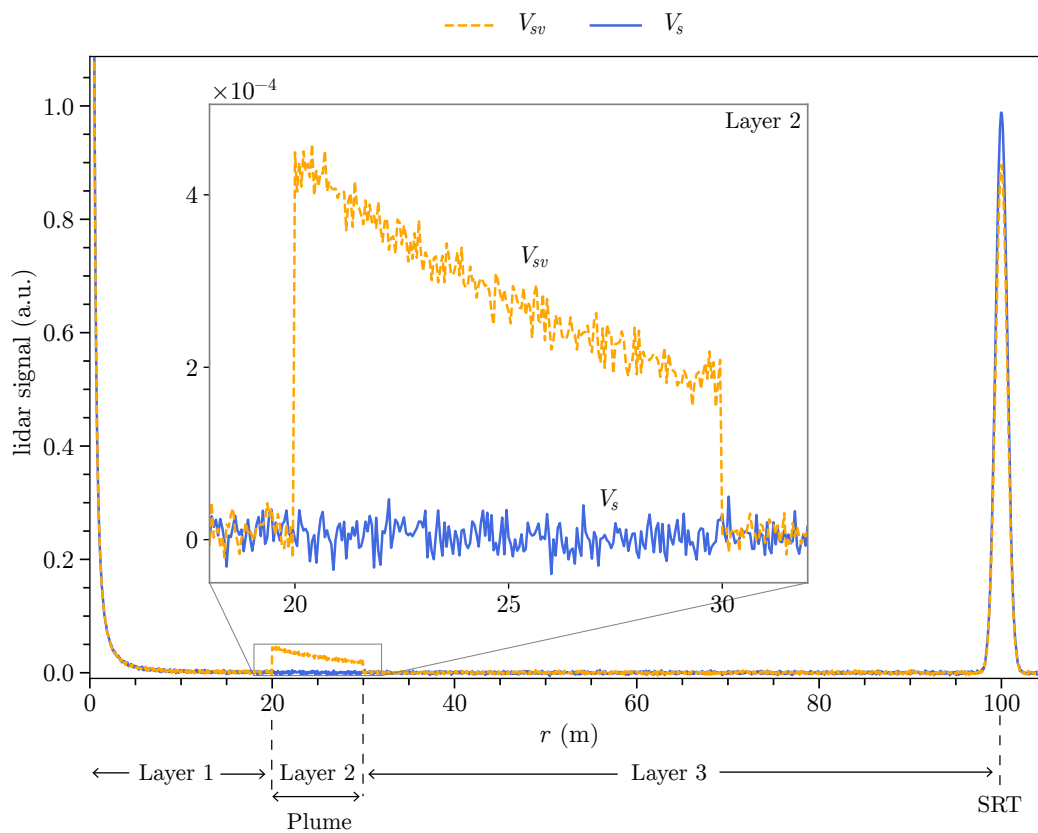


Figure 3. Theoretical noised lidar signals from a SRT V_s (blue line) and in the presence of an aerosol plume V_{sv} (orange dashed line). Simulations have been performed at 532 nm with molecular and continental aerosol background contributions.

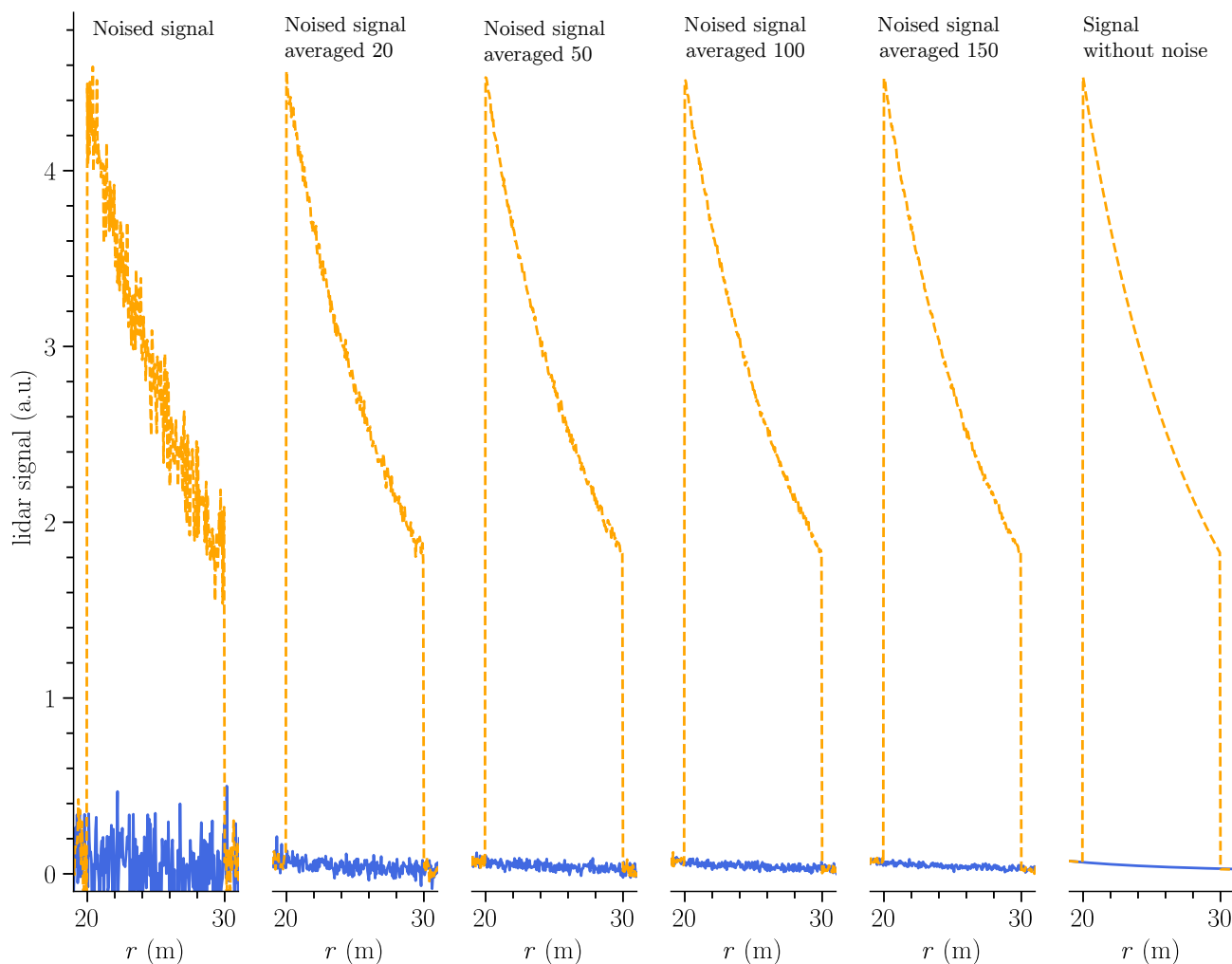


Figure 4. Lidar data sets used in the inversion method. In blue, (orange) the lidar signal in the absence (presence) of the volumetric media under study.

4.2 Noise impact on β_a and LR_a retrievals

200 LR_a is retrieved using Eq. 15. In addition to the six lidar-dataset described above, four different conditions of inversion are considered. In condition 1 the exact data of the background components are used as an input of the inversion algorithm. For conditions 2 and 3, β_b is over- and underestimated by 20% compared to the data used to generate the theoretical signals. In conditions 1 to 3, the inversion technique is performed over the entire signal range. Condition 4 is the same as condition 1, but the aerosol plume is spatially delimited. Table 2 summarizes the four-conditions for the six datasets. It is worth mentioning that



205 noised lidar signals obviously results in noised retrieved $\beta_a(r)$. Thus, to quantify the performance of the inversion technique, we consider the average value $\overline{\beta_a}$ of the plume. The retrieved value of LR_a can be directly compared to the theoretical value.

Conditions	1	2	3	4
Exact background constituents	X			X
$\beta_b + 20\%$		X		
$\beta_b - 20\%$			X	
Spatially bounded plume				X

Table 2. Conditions on the optical properties of the background components for the inversion method.

Figure 5 displays $\overline{\beta_a}$ for the six datasets and the four inversion conditions. It varies from 7.11×10^{-5} to $7.22 \times 10^{-5} \text{ m}^{-1} \cdot \text{sr}^{-1}$, which means an error of approximately 1% in comparison to the theoretical value. Conditions 2 and 3 result in a translation of the corresponding curve of $\pm 0.4\%$ with respect to the curve associated to condition 1, because of the over- and underestimation of 20% introduced in β_b . The performance is better for condition 4 whatever the dataset, since the maximum error is 0.5% for noised signals. The spatially bounded aerosol layer is often applied in inversion methods, and seem to herein improve the inversion method. For signal lidar without noise, $\overline{\beta_a}$ is not exactly equal to the theoretical value, maybe because of numerical computation errors in the inversion algorithm. Such a numerical error is about 0.12% (condition 1) and 0.04% (condition 4).

Fig. 6 is similar as Fig. 5 but considering LR_a . One obtains values ranging from 66 to 74 sr, with a maximum error of 5% compared to the theoretical value. In conditions 1, 2, and 3, using averaged noised signals has no consequence on the retrieved value of LR_a , contrary to what was obtained for $\overline{\beta_a}$. In condition 1, the maximum error is 2.1%. The graphs corresponding to conditions 2 and 3 are translated, with respect to the graph under to condition 1, by about $\pm 3\%$, and permuted respectively to the same but for $\overline{\beta_a}$. Nevertheless, the errors remain low with a maximum of 5% (condition 2) if 50 signals are averaged. However, under condition 4, the LR_a is much better for averaged signals and remains quite good for noisy signal (not averaged) with an error rate of 0.6%. Again, it seems that the spatial limitation of the plume increases the accuracy of the retrieval LR_a . Condition 1 remains however efficient for noised signals since deviation is below 2.1%. In the case of lidar signal without noise, the retrieved LR_a are not exactly equal to the theoretical LR_a ; numerical computation errors are about 0.13% (condition 1) and 0.05% (condition 4). An error of $\pm 20\%$ on β_b introduced initially will result in an under- or overestimation LR_a by $\pm 3\%$. Condition 4 is preferable to retrieve LR_a .

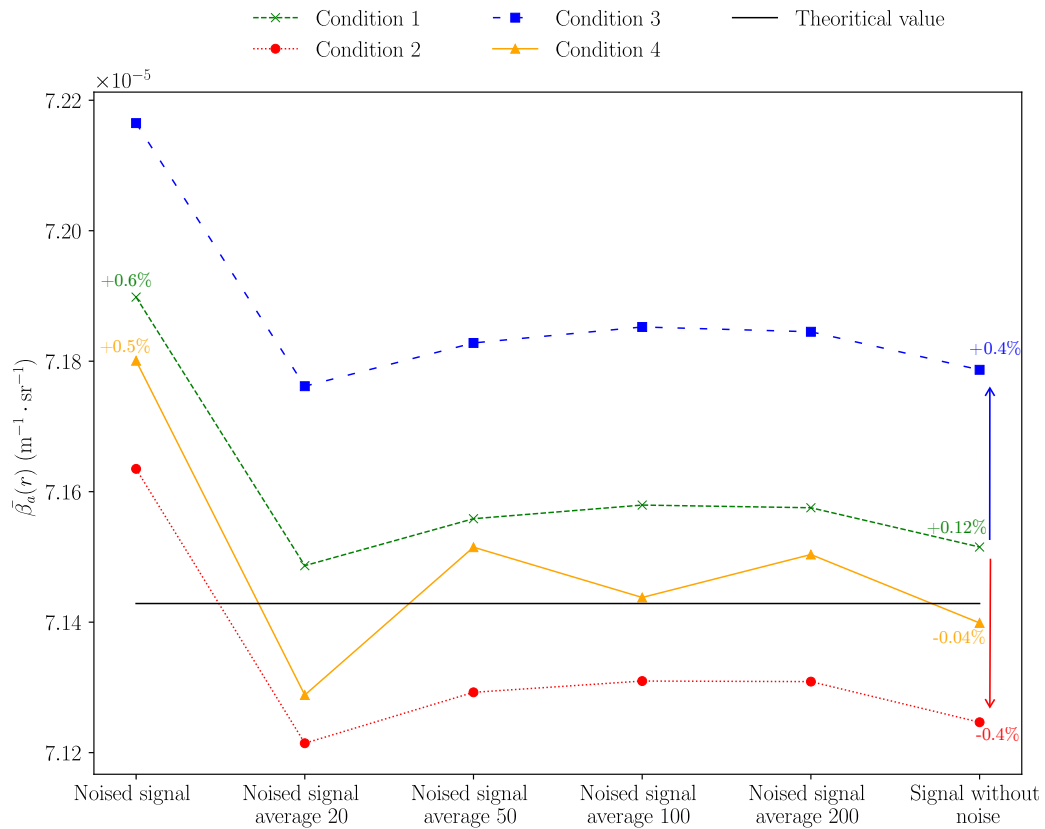


Figure 5. Retrieved $\bar{\beta}_a$ for six datasets and four different conditions of inversion.

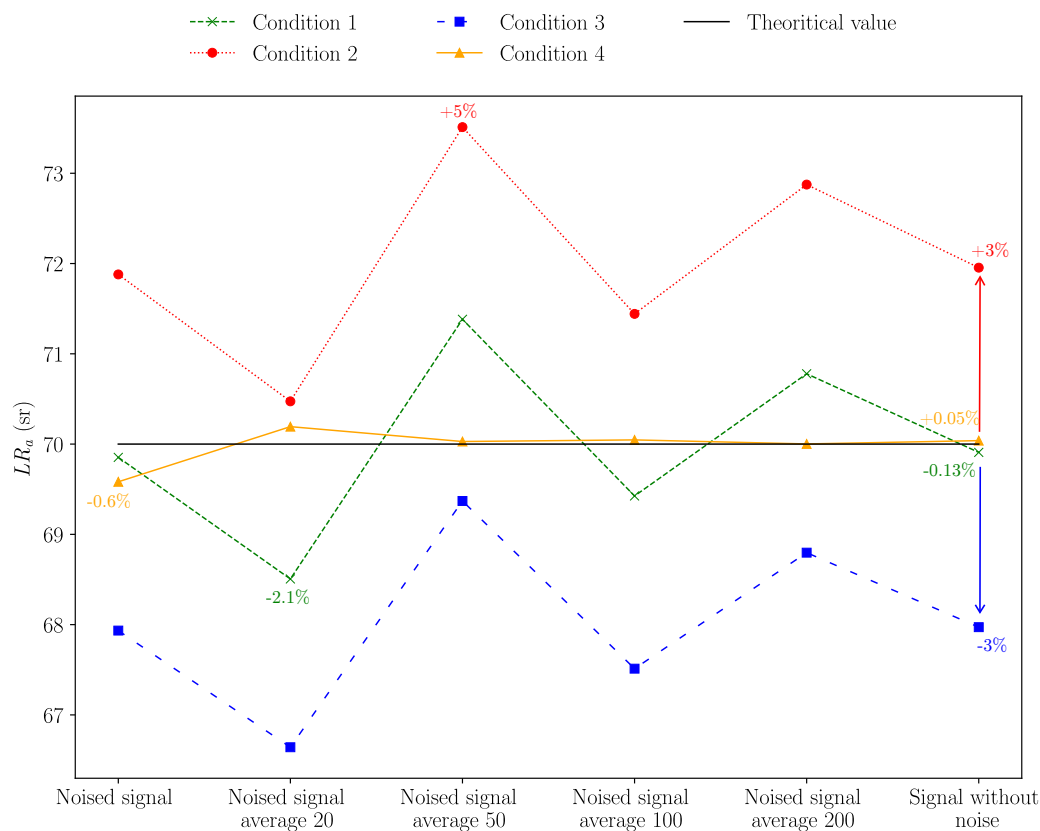


Figure 6. Retrieved LR_a for six datasets and four different conditions of inversion.

225 4.3 Plume optical property retrieval

The above study allowed us to test the new inversion method on noised signals, for different conditions of inversion, as a function of the number of signals averaged. Thereafter, lidar inversion is performed considering a spatially bounded plume and 100 signals for averaging. This last condition has been chosen because it corresponds to the number of signals available in less than 0.1 s with our lidar system (see Section 5). The theoretical results obtained by the inversion method with 100 averaged signals is also quite good (see above). Figure 9 displays the retrieved β_a if a theoretical lidar signal is introduced as a first guess. Table 3 lists the retrieved $\bar{\beta}_a$ and LR_a . Compared to theoretical values, errors are less than 0.7% for LR_a and below 0.1% for $\bar{\beta}_a$, although a peak of 2.2% is observed at $r = 28.8$ m.



	LR_a	$\bar{\beta}_a$
Value	70.05 sr	$7.14 \times 10^{-5} \text{ m}^{-1} \cdot \text{sr}^{-1}$
Error	0.07%	0.01%

Table 3. Plume optical property retrieved and associated errors

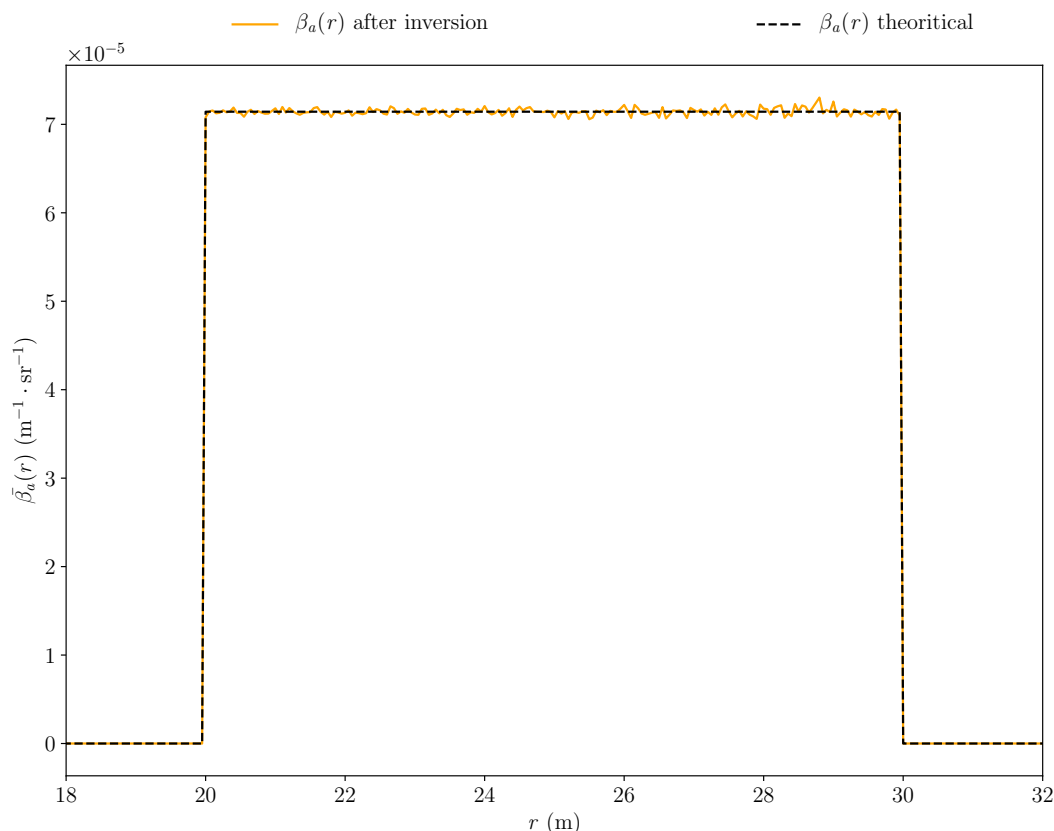


Figure 7. Retrieved $\beta_a(r)$ (orange solid line) for 100 theoretical averaged lidar signals and initial $\beta_a(r)$ (dark dashed line).

5 Case of real measurements

Our new inversion technique is now applied to real lidar measurements. The instrument used is named COLIBRIS² (Gaudfrin et al., 2018b)(Ceolato and Gaudfrin, 2018). This lidar is able to perform short-range measurements ($r_0 < 5$ m) at high spatial resolution (lower than 0.25 m). A Nd:YAG microchip laser source of the HORUS-LEUKOS company is used with a pulse energy peaking at 532 nm of 7.3 μJ and a repetition rate of 1 kHz. The backscattered light is collected by a Cassegrain telescope.

²Compact lidar for Broadband polarisation Spectral multi-Static measurement



In the detection part, a dichroic filter for the elastic channel is used before a photomultiplier tube. The signal is digitized at a sample frequency of 3 GHz after been amplified.

240 5.1 Description of the experimental operations

The lidar measurements are performed horizontally as illustrated in Fig. 8. The SRT is located 52 m away from the lidar instrument with $f_r = 0.20/\pi$. The mean laser beam direction is parallel to the normal of the surface. The laser source frequency and high-speed sampling allow to record more than 100 signals in 0.1 s (1 kHz). During this period, we assume that the environment does not evolve significantly. A first lidar measurement noted V_s is performed with the SRT and no plume. A
245 second measurement V_{sv} is then performed in the presence of an fog-oil plume at 38 m (thickness about 3.5 m).

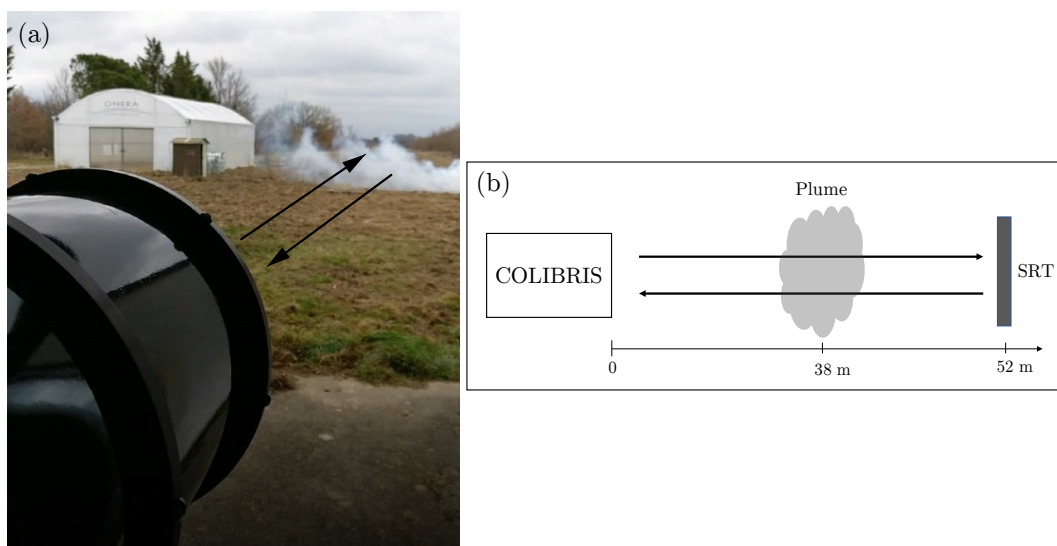


Figure 8. Experimental setup in an horizontal configuration. A fog-oil plume is generated between the lidar and the Lambertian SRT. (a) Photo and (b) illustration of the experimental setup with fog-oil plume.

The measured signals V_s and V_{sv} are shown on Fig. 9. In the presence of the oil plume, the backscatter peak of SRT is obviously weaker. During measurement, the pressure, temperature and visibility are respectively 1016 hPa, 288 K and 30 km. These data are used to compute β_b as described in Section 4.

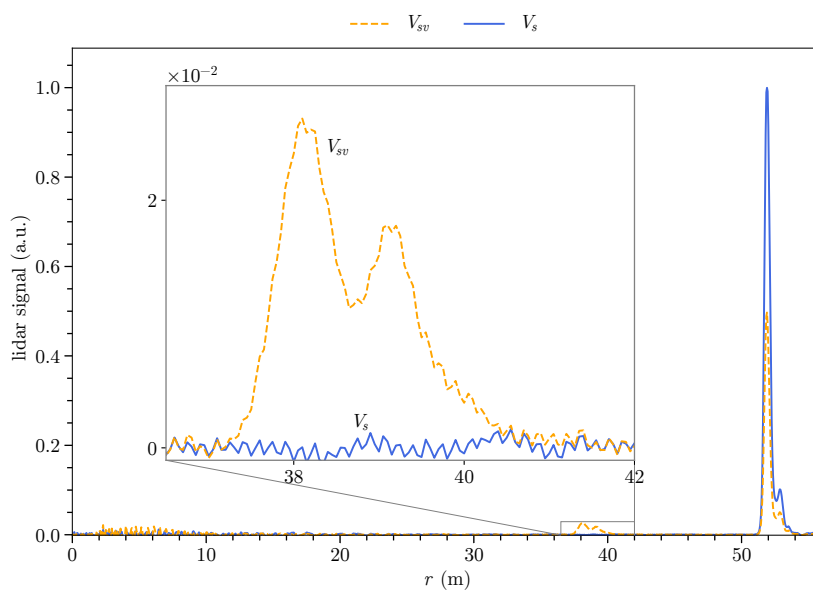


Figure 9. Lidar measurements of the experimental setup. In blue, (orange) the lidar signal in the absence (presence) of the oil-fog plume under study.

5.2 Optical property retrieval: fog-oil plume

250 The signals V_s and V_{sv} are used in the inversion procedure as described in Sections 3 and 4. The plume is spatially bounded (condition 4). The retrieved $\beta_a(r)$ is displayed in Fig. 10. In the densest range of the plume $\beta_a \approx 2 \times 10^{-3} \text{ m}^{-1} \text{ sr}^{-1}$. Also, the retrieved LR_a is around 98 sr. According to Bohlmann et al. (2018), this value corresponds, as expected, to smoke particles (at 532 nm, the lidar ratio ranges from 80 to 100 sr). The optical properties of the oil-fog plume of experimental retrieved with inverse method are summarized in Section 4.

255 The lidar signal reproduced from the retrieved $\beta_a(r)$, LR_a and of the instrumental constant deduced from the Eq. 14 gives a standard deviation from the exact value of 1.5×10^{-5} a.u. This shows the consistency and reliability of the new inversion method proposed in this paper.

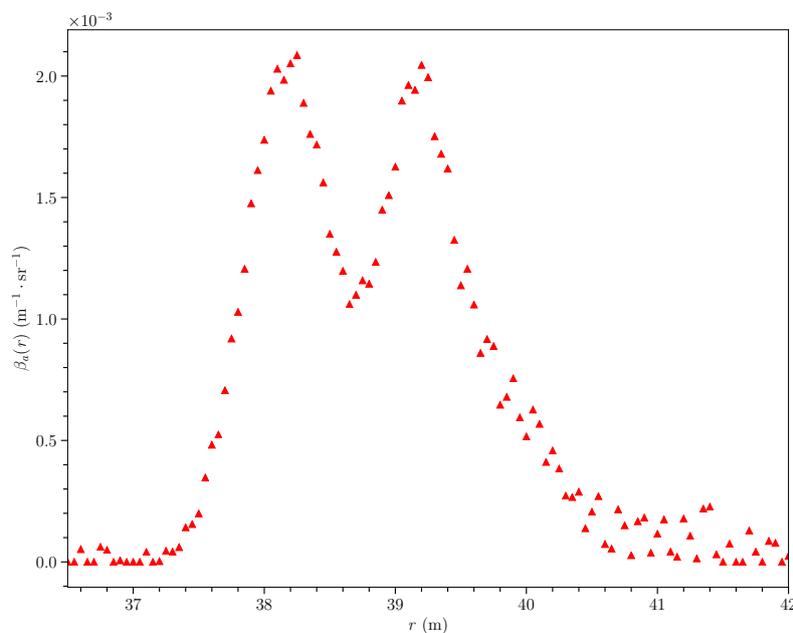


Figure 10. Retrieved $\beta_a(r)$ for real measurements with $LR_a = 98$ sr.

LR_a (sr $^{-1}$)	98
$\beta_{a,max}$ (m $^{-1}$ · sr $^{-1}$)	2.1×10^{-3}
$\alpha_{a,max}$ (m $^{-1}$)	2.1×10^{-1}
Optical thickness	3.6×10^{-1}

Table 4. Optical properties of oil-fog plume in experimental setup at 532 nm

6 Conclusions

In this paper, a new method has been introduced for lidar measurement inversion in a situation for which a volumetric layer (molecular Rayleigh scatterers) of the high troposphere is not available (*e.g.* airborne lidar observations, horizontal configuration of measurements). This method is based on a new expression of the lidar equation which allows us to use a surface reference target of a known BRDF instead of a volumetric one. This new formalism permits to invert short-range lidar measurements for which conventional inversion techniques can not directly be applied. Similarly to common inversion techniques, our method requires to introduce a background component (molecular and particulate contributions) that can be estimated either from radiative models or deduced from measurements of temperature, pressure, and visibility conditions.

Also, a new algorithm has been developed to retrieve, without any *a priori* assumptions relative to the medium to be characterized (aerosol plume), the backscattering coefficient (β_a) and lidar ratio (LR_a) of an aerosol plume, between the lidar and



the surface target reference. In other words, our technique method does not need to introduce any lidar ratio as an input for our inverse algorithm. For that, two lidar measurements are necessary: with and without the aerosol plume under consideration.
270 Comparing these two signals, one can retrieve the total extinction coefficient of the medium analysed and the instrumental constant of the lidar instrument. These two informations are used to constrain the inversion algorithm and finally to identify LR_a .

This algorithm has been first investigated using theoretical (simulated) lidar signals. The quality of the retrieval has been assessed by introducing noise in the simulated signals and by considering various conditions of inversion differing, in particular,
275 from one another according to the initial error introduced in the backscattering coefficient of the aerosol background. Thus, the robustness of algorithm has been shown, since in all the cases, the error on the retrieved values (*viz.* in β_a and LR_a) is less than 5%, at most. Also, we have found that inversion is better for spatially bounded aerosol plume.

The inversion algorithm has then been applied on real lidar short-range measurements of an oil-fog plume. The retrieved β_a and LR_a of the plume agree with values found in the literature for smoke-like particles. Moreover, thanks to the determination
280 of the instrumental constant, the measured signal has been computed from the inverted products, and an absolute error of 10^{-5} between the measure and the post-processed simulation has been encountered.

However, it is worth mentioning that the method proposed herein to find LR_a has some limitations. Precisely, it assumes that the medium under study is homogeneous and with a sufficient extinction coefficient. Indeed, since measurements are performed in the absence and in the presence of the medium, by means of a hard surface target of reference of known reflectance, the
285 algorithm converges less easily for very weakly diffusing plumes.

The new inversion technique presented in this paper suggests new airborne lidar applications, but it requires *a priori* knowledge of the referenced-target reflectance. Indeed, BRDF are often considered as Lambertian for natural targets (surface roughness, vegetation...), so it can be replaced by SRT reflectance. Applying this new inversion method therefore seems feasible and realistic. The evaluation of the method proposed in this paper, with considering the uncertainty of the target reflectance, has
290 not been performed, but it will be the topic of future researches papers.

7 Appendix

To solve Eq. 9, the exponential term can be written under another form. The method proposed by Vande Hey (2014) consists in integrating both members of the equation from r to r_s . So:

$$\int_r^{r_s} W(x) dx = \frac{c\tau}{2f_r F_{cor}} \frac{W(r_s)}{LR_a(r_s)} \int_r^{r_s} \left\{ Y(x) \exp \left[2 \int_x^{r_s} Y(r) dr \right] \right\} dx$$



Since:

$$\begin{aligned}
 \frac{d}{dx} \left\{ \exp \left[2 \int_x^{r_s} Y(r) dr \right] \right\} &= 2 \exp \left[2 \int_x^{r_s} Y(r) dr \right] \frac{d}{dx} \left[\int_x^{r_s} Y(r) dr \right] \\
 295 \qquad \qquad \qquad &= 2 \exp \left[2 \int_x^{r_s} Y(r) dr \right] \frac{d}{dx} [F(r_s) - F(x)] \\
 &= -2Y(x) \exp \left[2 \int_x^{r_s} Y(r) dr \right]
 \end{aligned}$$

where F is the primitive of Y , it ensues:

$$\begin{aligned}
 \int_r^{r_s} Y(x) \exp \left[2 \int_x^{r_s} Y(r) dr \right] dx &= -\frac{1}{2} \left\{ \exp \left[2 \int_x^{r_s} Y(r) dr \right] \right\}_r^{r_s} \\
 &= \frac{1}{2} \left\{ \exp \left[2 \int_r^{r_s} Y(r) dr \right] - 1 \right\}
 \end{aligned}$$

Therefore:

$$\int_r^{r_s} W(x) dx = \frac{c\tau}{4f_r F_{cor}} \frac{W(r_s)}{LR_a(r_s)} \left\{ \exp \left[2 \int_r^{r_s} Y(r) dr \right] - 1 \right\}$$

Finally, the exponential term becomes:

$$\exp \left[2 \int_r^{r_s} Y(r) dr \right] = 1 + \frac{4f_r F_{cor}}{c\tau} \frac{LR_a(r_s)}{W(r_s)} \left[\int_r^{r_s} W(r) dr \right]$$

300 *Competing interests.* The authors declare that they have no conflict of interest.

Acknowledgements. This research work has been performed within the framework of a CIFRE grant (ANRT) for the doctoral work of Florian Gaudfrin. The lidar systems has been funded by the PROMETE project (ONERA). The laser source used in this paper for the experimental setup has been designed by Benoit Faure, Paul-Henri Pioget, and Guillaume Huss from the company HORUS-LEUKOS.



References

- 305 Estimates of the direct and indirect radiative forcing due to tropospheric aerosols: A review, *Reviews of Geophysics*, 38, 513–543, <https://doi.org/10.1029/1999RG000078>, 2000.
Journal of Geophysical Research D: Atmospheres, 110, 1–13, <https://doi.org/10.1029/2004JD005124>, 2005.
Combined Determination of the Chemical Composition and of Health Effects of Secondary Organic Aerosols: The POLYSOA Project, *Journal of Aerosol Medicine and Pulmonary Drug Delivery*, 21, 145–154, <https://doi.org/10.1089/jamp.2007.0655>, 2008.
- 310 Ackermann, J.: The extinction-to-backscatter ratio of tropospheric aerosol: A numerical study, *Journal of Atmospheric and Oceanic Technology*, 15, 1043–1050, [https://doi.org/10.1175/1520-0426\(1998\)015<1043:TETBRO>2.0.CO;2](https://doi.org/10.1175/1520-0426(1998)015<1043:TETBRO>2.0.CO;2), 1998.
Anon: U.S. Standard Atmosphere, Tech. rep., NASA, Washington, DC, United States, 1976.
Ansmann, A., Riebesell, M., and Weitkamp, C.: Measurement of atmospheric aerosol extinction profiles with a Raman lidar, *Optics Letters*, 15, 746, <https://doi.org/10.1364/OL.15.000746>, 1990.
- 315 Ansmann, A., Wandinger, U., Riebesell, M., Weitkamp, C., and Michaelis, W.: Independent measurement of extinction and backscatter profiles in cirrus clouds by using a combined Raman elastic-backscatter lidar, *Applied Optics*, 31, 7113, <https://doi.org/10.1364/AO.31.007113>, 1992.
Ansmann, A., Neuber, R., Rairoux, P., and Wandinger, U.: *Advances in Atmospheric Remote Sensing with Lidar*, vol. 34, Springer Berlin Heidelberg, Berlin, Heidelberg, <https://doi.org/10.1007/978-3-642-60612-0>, 1997.
- 320 Ansmann, A., Baldasano, J., Calpini, B., Chaikovsky, Anatoly and Flamant, P., Mitev, V., Papayannis, A., Pelon, J., Resendes, D., Schneider, J., Trickl, T., and Vaughan, G.: EARLINET: A European Aerosol Research Lidar Network, Tech. rep., 2001.
Berk, A., Acharya, P., and Bernstein, L.: Band model method for modeling atmospheric propagation at arbitrarily fine spectral resolution, 2008.
Berk, A., Conforti, P., Kennett, R., Perkins, T., Hawes, F., and van den Bosch, J.: MODTRAN6: a major upgrade of the MODTRAN radiative transfer code, vol. 9088, p. 90880H, International Society for Optics and Photonics, <https://doi.org/10.1117/12.2050433>, 2014.
- 325 Bissonnette, L. R.: Multiple-scattering lidar equation, *Applied Optics*, 35, 6449, <https://doi.org/10.1364/AO.35.006449>, 1996.
Bodhaine, B. A., Wood, N. B., Dutton, E. G., and Slusser, J. R.: On Rayleigh Optical Depth Calculations, *Journal of Atmospheric and Oceanic Technology*, 16, 1854–1861, [https://doi.org/10.1175/1520-0426\(1999\)016<1854:ORODC>2.0.CO;2](https://doi.org/10.1175/1520-0426(1999)016<1854:ORODC>2.0.CO;2), 1999.
Bohmann, S., Baars, H., Radenz, M., Engelmann, R., and Macke, A.: *Atmospheric Chemistry and Physics*, 18, 9661–9679, <https://doi.org/10.5194/acp-18-9661-2018>, 2018.
- 330 Bucholtz, A.: Rayleigh-scattering calculations for the terrestrial atmosphere, *Applied Optics*, 34, 2765, <https://doi.org/10.1364/AO.34.002765>, 1995.
Bufton, J. L.: Laser Altimetry Measurements from Aircraft and Spacecraft, *Proceedings of the IEEE*, 77, 463–477, <https://doi.org/10.1109/5.24131>, 1989.
- 335 Ceolato, R. and Gaudfrin, F.: Short-range characterization of freshly emitted carbonaceous particles by LiDAR, in: General Meeting, Nafplio, 2018.
Ceolato, R., Gaudfrin, F., Pujol, O., Riviere, N., Berg, M. J., and Sorensen, C. M.: Lidar cross-sections of soot fractal aggregates: Assessment of equivalent-sphere models, *Journal of Quantitative Spectroscopy and Radiative Transfer*, 212, 39–44, <https://doi.org/10.1016/j.jqsrt.2017.12.004>, 2018.



- 340 Clark, W. E. and Whitby, K. T.: Concentration and Size Distribution Measurements of Atmospheric Aerosols and a Test of the Theory of Self-Preserving Size Distributions, *Journal of the Atmospheric Sciences*, 24, 677–687, [https://doi.org/10.1175/1520-0469\(1967\)024<0677:CASDMO>2.0.CO;2](https://doi.org/10.1175/1520-0469(1967)024<0677:CASDMO>2.0.CO;2), 1967.
- Collis, R. T. H. and Russell, P. B.: Lidar measurement of particles and gases by elastic backscattering and differential absorption, pp. 71–151, https://doi.org/10.1007/3-540-07743-X_18, 1976.
- 345 Comeron, A., Sicard, M., Kumar, D., and Rocadenbosch, F.: Use of a field lens for improving the overlap function of a lidar system employing an optical fiber in the receiver assembly, *Applied Optics*, 50, 5538, <https://doi.org/10.1364/AO.50.005538>, 2011.
- DeMott, P. J., Prenni, A. J., Liu, X., Kreidenweis, S. M., Petters, M. D., Twohy, C. H., Richardson, M. S., Eidhammer, T., and Rogers, D. C.: Predicting global atmospheric ice nuclei distributions and their impacts on climate, *Proceedings of the National Academy of Sciences*, 107, 11 217–11 222, <https://doi.org/10.1073/pnas.0910818107>, 2010.
- 350 Elias, T., Haeffelin, M., Drobinski, P., Gomes, L., Rangognio, J., Bergot, T., Chazette, P., Raut, J. C., and Colomb, M.: Particulate contribution to extinction of visible radiation: Pollution, haze, and fog, *Atmospheric Research*, 92, 443–454, <https://doi.org/10.1016/j.atmosres.2009.01.006>, 2009.
- Fernald, F. G.: Analysis of atmospheric lidar observations: some comments, *Applied Optics*, 23, 652, <https://doi.org/10.1364/ao.23.000652>, 1984.
- 355 Fernald, F. G., Herman, B. M., and Reagan, J. A.: Determination of Aerosol Height Distributions by Lidar, *Journal of Applied Meteorology*, 11, 482–489, [https://doi.org/10.1175/1520-0450\(1972\)011<0482:DOAHDB>2.0.CO;2](https://doi.org/10.1175/1520-0450(1972)011<0482:DOAHDB>2.0.CO;2), 1972.
- Finlayson-Pitts, B. J. and Pitts, J. N. J.: *The Atmospheric System, Chemistry of the Upper and Lower Atmosphere: Theory, Experiments, and Applications*, pp. 15–42, <https://doi.org/10.1016/B978-012257060-5/50004-6>, 2000.
- Gaudfrin, F., Ceolato, R., Pujol, O., Riviere, N., and Hu, Q.: Supercontinuum lidar for hydrometeors and aerosols optical properties determination, in: *EGU General Assembly 2018*, vol. 20, p. 14436, 2018a.
- 360 Gaudfrin, F., Ceolato, R., Riviere, N., Pujol, O., and Huss, G.: New technics to probe aerosols radiative properties from visible to infrared, in: *The 13th International IR Target and Background Modeling & Simulation Workshop*, Banyuls-sur-Mer, 2018b.
- Gaudfrin, F., Ceolato, R., Pujol, O., and Riviere, N.: A new-lidar inversion technique using a surface reference target at short - range, in: *The 29th International Laser Radar Conference*, pp. 3–6, Hefei, 2019.
- 365 Glickman, T. and Zenk, W.: *Glossary of Meteorology*, American Meteorological Society, Boston, 855 pp. 2, 2000.
- Hadamard, J.: Théorie des équations aux dérivées partielles linéaires hyperboliques et du problème de Cauchy, *Acta Mathematica*, 31, 333–380, <https://doi.org/10.1007/BF02415449>, 1908.
- Hall, F. F. and Ageo, H. Y.: Absolute calibration of a laser system for atmospheric probing, *Applied Optics*, 9, 1820–1824, <https://doi.org/10.1364/AO.9.001820>, 1970.
- 370 Halldórsson, T. and Langerholc, J.: Geometrical form factors for the lidar function, *Applied Optics*, 17, 240, <https://doi.org/10.1364/AO.17.000240>, 1978.
- Hansen, J., Sato, M., and Ruedy, R.: Radiative forcing and climate response, *Journal of Geophysical Research: Atmospheres*, 102, 6831–6864, <https://doi.org/10.1029/96JD03436>, 1997.
- Hess, M., Koepke, P., Schult, I., Hess, M., Koepke, P., and Schult, I.: Optical Properties of Aerosols and Clouds: The Software Package OPAC, *Bulletin of the American Meteorological Society*, 79, 831–844, [https://doi.org/10.1175/1520-0477\(1998\)079<0831:OPOAAC>2.0.CO;2](https://doi.org/10.1175/1520-0477(1998)079<0831:OPOAAC>2.0.CO;2), 1998.



- Hoff, R. M., Bösenberg, J., and Pappalardo, G.: The GAW Aerosol Lidar Observation Network (GALION), in: International Geoscience and Remote Sensing Symposium (IGARSS-08), Boston (USA), pp. 6–11, 2008.
- Horvath, H.: On the applicability of the Koschmieder visibility formula, 5, 177–184, [https://doi.org/10.1016/0004-6981\(71\)90081-3](https://doi.org/10.1016/0004-6981(71)90081-3), 1971.
- 380 Hyslop, N. P.: Impaired visibility: the air pollution people see, *Atmospheric Environment*, 43, 182–195, <https://doi.org/10.1016/j.atmosenv.2008.09.067>, 2009.
- Jäger, H.: Long-term record of lidar observations of the stratospheric aerosol layer at Garmisch-Partenkirchen, *Journal of Geophysical Research D: Atmospheres*, 110, 1–9, <https://doi.org/10.1029/2004JD005506>, 2005.
- Klett, J. D.: Stable analytical inversion solution for processing lidar returns, *Applied Optics*, 20, 211, <https://doi.org/10.1364/AO.20.000211>,
385 1981.
- Klett, J. D.: Lidar inversion with variable backscatter/extinction ratios, *Applied Optics*, 24, 1638, <https://doi.org/10.1364/AO.24.001638>, 1985.
- Kraft, D.: Software Package for Sequential Quadratic Programming, 1988.
- Kumar, D. and Rocadenbosch, F.: Determination of the overlap factor and its enhancement for medium-size tropospheric lidar systems: a
390 ray-tracing approach, *Journal of Applied Remote Sensing*, 7, 073 591, <https://doi.org/10.1117/1.JRS.7.073591>, 2013.
- Labarre, L., Caillault, K., Fauqueux, S., Malherbe, C., Roblin, A., Rosier, B., and Simoneau, P.: An overview of MATISSE-v2.0, p. 782802, <https://doi.org/10.1117/12.868183>, 2010.
- Leblanc, T., Trickl, T., and Vogelmann, H.: Lidar, vol. 102 of *Springer Series in Optical Sciences*, Springer-Verlag, New York, <https://doi.org/10.1007/b106786>, 2005.
- 395 Li, J., Gong, W., and Ma, Y.: Atmospheric Lidar Noise Reduction Based on Ensemble Empirical Mode Decomposition, IS-PRS - International Archives of the Photogrammetry, Remote Sensing and Spatial Information Sciences, XXXIX-B8, 127–129, <https://doi.org/10.5194/isprsarchives-XXXIX-B8-127-2012>, 2012.
- Mao, F., Gong, W., and Li, C.: Anti-noise algorithm of lidar data retrieval by combining the ensemble Kalman filter and the Fernald method, *Optics Express*, 21, 8286, <https://doi.org/10.1364/OE.21.008286>, 2013.
- 400 Matsumoto, M. and Takeuchi, N.: Effects of misestimated far-end boundary values on two common lidar inversion solutions, *Applied Optics*, 33, 6451, <https://doi.org/10.1364/AO.33.006451>, 1994.
- Mattis, I., Ansmann, A., Müller, D., Wandinger, U., and Althausen, D.: Multilayer aerosol observations with dual-wavelength Raman lidar in the framework of EARLINET, *Journal of Geophysical Research D: Atmospheres*, 109, 1–15, <https://doi.org/10.1029/2004JD004600>, 2004.
- 405 Pedrós, R., Estellés, V., Sicard, M., Gómez-Amo, J. L., Utrillas, M. P., Martínez-Lozano, J. A., Rocadenbosch, F., Pérez, C., and Recio Baldasano, J. M.: Climatology of the aerosol extinction-to-backscatter ratio from sun-photometric measurements, *IEEE Transactions on Geoscience and Remote Sensing*, 48, 237–249, <https://doi.org/10.1109/TGRS.2009.2027699>, 2010.
- Popovicheva, O. B., Engling, G., Ku, I.-T., Timofeev, M. A., and Shonija, N. K.: Aerosol Emissions from Long-Lasting Smoldering of Boreal Peatlands: Chemical Composition, Markers, and Microstructure, *Aerosol and Air Quality Research*, 2, 213–218,
410 <https://doi.org/10.4209/aaqr.2018.08.0302>, 2019.
- Rocadenbosch, F., Frasier, S., Kumar, D., Lange Vega, D., Gregorio, E., and Sicard, M.: Backscatter error bounds for the elastic lidar two-component inversion algorithm, *IEEE Transactions on Geoscience and Remote Sensing*, 50, 4791–4803, <https://doi.org/10.1109/TGRS.2012.2194501>, 2012.



- Sasano, Y., Browell, E. V., and Ismail, S.: Error caused by using a constant extinction/backscattering ratio in the lidar solution, *Applied Optics*, 24, 3929, <https://doi.org/10.1364/AO.24.003929>, 1985.
- 415
- Sicard, M., Chazette, P., Pelon, J., Won, J., and Yoon, S.-C.: Variational method for the retrieval of the optical thickness and the backscatter coefficient from multiangle lidar profiles, *Applied Optics*, 41, 493–502, <https://doi.org/10.1364/AO.41.000493>, 2002.
- Simoneau, P., Berton, R., Caillault, K., Durand, G., Huet, T., Labarre, L., Malherbe, C., Miesch, C., Roblin, A., and Rosier, B.: MATISSE: advanced Earth modeling for imaging and scene simulation, in: *Proceedings of SPIE*, edited by Kohnle, A., Gonglewski, J. D., and
- 420
- Schmugge, T. J., vol. 4538, p. 39, <https://doi.org/10.1117/12.454410>, 2002.
- Stelmaszczyk, K., Dell’Aglia, M., Chudzyński, S., Staciewicz, T., and Wöste, L.: Analytical function for lidar geometrical compression form-factor calculations, *Applied Optics*, 44, 1323, <https://doi.org/10.1364/AO.44.001323>, 2005.
- Sun, X.: *Lidar Sensors From Space*, Elsevier, <https://doi.org/10.1016/B978-0-12-409548-9.10327-6>, 2018.
- Swinehart, D.: The Beer-Lambert law, *Journal of Chemical Education*, 39, 335, <https://doi.org/10.1021/ed039p333>, 1962.
- 425
- Vande Hey, J., Coupland, J., Foo, M. H., Richards, J., and Sandford, A.: Determination of overlap in lidar systems, *Applied Optics*, 50, 5791, <https://doi.org/10.1364/AO.50.005791>, 2011.
- Vande Hey, J. D.: Theory of Lidar, pp. 23–41, https://doi.org/10.1007/978-3-319-12613-5_2, 2014.
- Vargas-Ubera, J., Aguilar, J. F., and Gale, D. M.: Reconstruction of particle-size distributions from light-scattering patterns using three inversion methods, *Applied Optics*, 46, 124, <https://doi.org/10.1364/AO.46.000124>, 2007.
- 430
- Wandinger, U. and Ansmann, A.: Experimental determination of the lidar overlap profile with Raman lidar, *Applied Optics*, 41, 511–514, <https://doi.org/10.1364/AO.41.000511>, 2002.
- Zhang, J., Wei, E., Wu, L., Fang, X., Li, F., Yang, Z., Wang, T., and Mao, H.: Elemental Composition and Health Risk Assessment of PM₁₀ and PM_{2.5} in the Roadside Microenvironment in Tianjin, China, *Aerosol and Air Quality Research*, 18, 1817–1827, <https://doi.org/10.4209/aaqr.2017.10.0383>, 2018.